HHS Public Access

Author manuscript

Connect Tissue Res. Author manuscript; available in PMC 2018 May 01.

Published in final edited form as:

Connect Tissue Res. 2017 ; 58(3-4): 373–385. doi:10.1080/03008207.2016.1251425.

Quantitative histological grading methods to assess subchondral bone and synovium changes subsequent to medial meniscus transection in the rat

Heidi E. Kloefkorn and **Kyle D. Allen**

J. Crayton Pruitt Family Department of Biomedical Engineering, University of Florida, Gainesville, FL, USA

Abstract

Aim of the Study—The importance of the medial meniscus to knee health is demonstrated by studies which show meniscus injuries significantly increase the likelihood of developing osteoarthritis (OA), and knee OA can be modeled in rodents using simulated meniscus injuries. Traditionally, histological assessments of OA in these models have focused on damage to the articular cartilage; however, OA is now viewed as a disease of the entire joint as an organ system. The aim of this study was to develop quantitative histological measures of bone and synovial changes in a rat medial meniscus injury model of knee OA.

Materials and Methods—To initiate OA, a medial meniscus transection (MMT) and a medial collateral ligament transection (MCLT) were performed in 32 male Lewis rats (MMT group). MCLT alone served as the sham procedure in 32 additional rats (MCLT sham group). At weeks 1, 2, 4, and 6 post-surgery, histological assessment of subchondral bone and synovium was performed (n = 8 per group per time point).

Results—Trabecular bone area and the ossification width at the osteochondral interface increased in both the MMT and MCLT groups. Subintimal synovial cell morphology also changed in MMT and MCLT groups relative to naïve animals.

Conclusions—OA affects the joint as an organ system, and quantifying changes throughout an entire joint can improve our understanding of the relationship between joint destruction and painful OA symptoms following meniscus injury.

Keywords

Meniscus injury; osteoarthritis; quantitative histology; subchondral bone; subintima; synovium

CONTACT: Kyle D. Allen, kyle.allen@bme.ufl.edu, J Crayton Pruitt Family Department of Biomedical Engineering, University of Florida, 1275 Center Drive, Biomedical Sciences Building, J389, Gainesville, FL 32610, USA. Tel: +(352) 273-9337.

Color versions of one or more of the figures in this article can be found online at http://www.tandfonline.com/icts.

Declaration of interest

The authors report no conflicts of interest. The content is solely the responsibility of the authors and does not necessarily represent the official views of the National Institutes of Health or the University of Florida.

Introduction

The importance of the medial meniscus to knee health is demonstrated by studies showing meniscus injuries significantly increase the likelihood of developing osteoarthritis (OA) (1,2). While some hypothesize OA after meniscal injury proceeds solely due to changes in load distribution (3), the maladaptive repair response observed in OA is generally thought to result from biological responses occurring throughout the entire joint (4). In rodent preclinical OA models, surgically simulated meniscus damage can be used to model post-traumatic OA development in the meniscus-deficient joint (5,6). Moreover, histological evidence of joint damage following simulated meniscal injury in the rat and mouse emulates several clinical features of knee OA, such as focal cartilage lesions and osteophyte formation.

In rodent meniscal injury models, joint damage is traditionally evaluated through histological grading, with the most prevalent grading systems originating from the Mankin scheme. In addition to Mankin-based systems, the Osteoarthritis Research Society International (OARSI) recommended histological assessment methods for specific animals in 2010 (7–10). For the rat, the OARSI histological assessment method emphasizes quantitative measures of cartilage damage, with a few supporting qualitative ranks (7). However, none of these systems fully assess other joint changes (11–13).

Since damage occurs throughout the joint, the inclusion of multiple tissues in the grading process may improve our evaluation of OA progression. For example, cartilage lesions are a significant effect of OA; however, damage to cartilage can also alter joint mechanics and result in remodeling of the subchondral bone (14–16). Likewise, cartilage fragments can incite an inflammatory response in the synovium (17). Thus, multiple tissues communicate and adapt through complex feedback loops; and because one tissue cannot change in isolation, histological measures that quantify changes throughout the joint may complement existing cartilage measures and provide a more complete picture of the OA process.

The objective of this study was to develop quantitative histological measures of bone and synovium following a simulated meniscal injury in the rat. First, using a quantitative histological grading philosophy similar to that of OARSI scheme, measures of histological changes in the subchondral bone and synovium were developed. Then, these measures were applied to histological sections of rat knee OA at 1, 2, 4, and 6 weeks after surgical simulation of a complete radial meniscal tear. Our data demonstrate that, along with cartilage damage, subchondral bone trabecular and ossification areas increased progressively after a simulated meniscal injury. However, the same subchondral bone remodeling was observed with medial collateral ligament (MCL) transection alone (sham procedure), despite no evidence of cartilage damage. Moreover, cell morphology in the synovial subintimal layer was altered with simulated meniscal injury; and while cellular changes in the synovium were also observed with MCL transection, the relative severity of synovial changes with meniscal injury was much greater than that of MCL alone.

Methods

Experimental design

All procedures were performed according to the University of Florida Institutional Animal Care and Use Committee (IACUC), the Association for Assessment and Accreditation of Laboratory Animal Care (AAALAC), and National Institutes of Health (NIH) guidelines. To be clear, surgery, mechanical sensitivity testing, spatiotemporal gait analysis, and OARSI histopathology grading have been previously reported for the animals included in this study (18). The aim of this study was to develop and assess previously unmeasured histological features in bone and synovium following meniscal injury in the rat.

Rat medial meniscus injury model

To model a meniscal injury, 72 male Lewis rats (3 months, 250 g) were obtained from Charles River Laboratories and allowed to acclimate to the housing at the University of Florida for at least one week prior to any testing. An MCL transection followed by a medial meniscus transection (MMT) was performed on 32 animals, as previously described (5). Briefly, anesthesia was induced with 3–5% isoflurane, with anesthesia maintained with 1–2% isoflurane via mask inhalation. The knee was prepped for aseptic surgery using povidone-iodine and ethanol in triplicate, followed by a final application of povidone-iodine. A medial skin incision was made along the knee, and tissue was bluntly dissected to expose the MCL. The MCL was transected (MCLT) and the joint was placed in a valgus orientation to expose the medial meniscus. The meniscus was then transected radially with an 11 blade scalpel (MMT). In addition, 32 animals received only MCLT, but without meniscal injury (MCLT sham). Please note, prior work by several groups has demonstrated that MCLT alone does not result in cartilage damage over 4–5 weeks and is frequently referred to as the sham procedure for the rat MMT model (5,6,18–21). The incisions of animals tested at week 1 post-surgery were closed using interrupted 5-0 Vicryl sutures. In the 2, 4, and 6 week post-surgery groups, wounds were closed using 9 mm wound clips, which were subsequently removed at 10–14 days after surgery. Because gait analysis was performed on these animals for a separate study (18), this difference in closure techniques was selected to reduce gait modifications caused by the external wound clips at 1 week post-surgery. The eight remaining animals served as a naïve cohort.

Histology

At 1, 2, 4, and 6 weeks after surgery, animals were humanely euthanized. Knees were dissected and fixed for 48 hours in 10% neutral buffered formalin (Fisher Scientific, Waltham, MA). Ranging from 18 to 25 days, joints were decalcified at 4 °C in Cal-Ex (Fisher Scientific), with decalcification reagent exchanged every 48 hours until the bone was soft. The joints were then processed for paraffin embedding via vacuum infiltration. Paraffin-embedded joints were sectioned frontally on a rotary microtome (Leica Biosystems, Buffalo Grove, IL, RM2255) at a thickness of 10 μm per section. The sections were collected in strips of 10 (representing a total thickness of 100 μm), with 3–5 sequential sections mounted onto each slide with the rest of the strip discarded. Thus, each slide represents joint changes at approximately every 100 μm.

Histological images

Slides representing structural damage to the articular cartilage were stained with toluidine blue, and the medial compartment of each section was imaged at 4× magnification on an EVOS XL Core (Fisher Scientific). A total of 9 medial compartment images were taken of 3 consecutive sections from each of the 3 sequential slides (i.e. 3 histological sections from the slide representing the most significant cartilage damage and 3 histological sections from a slide 100 μm anterior and 100 μm posterior from the slide representing the most significant cartilage damage). Using the location guidelines for synovial thickness recommended by the OARSI histopathology initiative for the rat, one additional image of the medial, proximal synovium (between the meniscal and bony attachments) was taken at 10× magnification from the section representing the most significant cartilage damage. Prior to grading, the histological images were randomized to blind the grader. All histological measures and the section(s) where the measure was conducted are described below and in Table 1.

Ossification at the subchondral bone–cartilage interface

Using the image representing the most severe cartilage damage, measurement of bony changes at the subchondral bone–cartilage interface was calculated by four blinded graders using a MATLAB-based graphic user interface available for download at the corresponding author's website (GEKO-Subchondral Bone, Figure 1, http://www.orthobme.com/resources.html).

To quantify subchondral bone ossification, each grader first estimates the medial and lateral endpoints of the tibial osteochondral interface (Figure 1, black bar). Then, the grader traces the osteochondral interface of the ossified cartilage (yellow area). The script uses these coordinates to estimate the width and height of subchondral bone ossification as ratios of the osteochondral interface width.

Subchondral bone edema

In the nine medial compartment histological images from each knee (spacing described above), the four graders were asked to trace areas representing subchondral bone edema, if present (pink area, Figure 1). If an edema was present on an image, the image was assigned a value of 1; otherwise, the image was assigned a value of 0 (indicating no edema was present on that image). For each animal, the percentage of the nine sections containing evidence of edema was calculated. In addition, edema size was calculated, when present.

Epiphyseal trabecular bone area

Using recommendations from the American Society for Bone and Mineral Research (ASBMR) standard and the 2012 updated ASBMR recommendations for two-dimensional (2-D) bone histomorphometry (22,23), epiphyseal trabecular bone area (ETBA) was calculated by two blinded graders. However, while the ASBMR standard describes each component of the recommended equations, this standard does not provide detailed guidelines on how to measure each component. For example, the ASBMR trabecular bone volume standard is defined as trabecular bone volume divided by total bone volume (trabecular bone volume plus bone marrow voids), but no specific method is suggested to collect trabecular bone volume or total bone volume, such as the number of 2-D histological

slides which should be evaluated, nor the spacing between these slides. As such, we use the term epiphyseal trabecular bone area in this manuscript, such that it is clear these measures are coming from 2-D histological sections, similar to previous reports of trabecular bone area (TBA) (16,24).

To calculate subchondral ETBA, the nine medial compartment histological images from each knee (spacing described above) were first prepared in Adobe Photoshop CS5.1. Here, the image was rotated such that the tibial plateau was approximately horizontal, and the image was cropped to eliminate unused portions of the image. In addition, tissues not presenting the subchondral trabecular bone and bone marrow voids were filled in as black (Figure 2A). This edit eliminated tibial articular cartilage and pre-osteophytes. Subsequently, any point where the dehydrated bone marrow touched subchondral bone was erased in order to isolate the bone marrow voids from the trabecular bone. Images prepared in Photoshop were then loaded into a MATLAB script, which automatically removes dehydrated bone marrow using object and color filters and calculates the number of bone marrow voids, size of bone marrow voids, and ETBA over the entire subchondral bone area (Figure 2B, available for download at the corresponding author's website, GEKO-Subchondral Bone, http://www.orthobme.com/resources.html). Additionally, the script subdivides the ETBA into a 3 × 3 grid and calculates the ETBA in each zone (Figure 2b).

Trabecular bone area

In addition to ETBA, a more isolated TBA measure was also calculated. TBA is a representation of the amount of subchondral trabecular bone excluding the portions of bone between the tibial plateau cartilage and the bone marrow spaces and the portions of bone between the epiphyseal plane and bone marrow space (Figure 2A). The images used to measure TBA were created by taking the ETBA images described above and removing additional trabecular bone such that the TBA could be measured only where bone marrow spaces are included. Once these TBA images were created, they were processed by the same MATLAB script as mentioned above.

Synovial subintima

To assess changes in the synovial subintima, four blinded graders used the 10× magnification image of the synovium to identify a portion of synovium proximal to the medial meniscus but distal from the synovium's connection to the femur in which the subintimal cells were visible and aligned (Figure 3A). Once the desired portion of synovium was identified, each grader cropped the 10× magnification image of the synovium in Adobe Photoshop CS5.1 to isolate the desired portion of synovium (Figure 3B). The Photoshop altered image was rotated to align the image edge with the edge of the synovium and then loaded into a MATLAB script to assess the subintimal cell density, aspect ratio, and alignment (Figure 3C, available for download at the corresponding author's website, GEKO-Subchondral Bone, http://www.orthobme.com/resources.html).

Since toluidine blue is metachromatic and has an affinity for nucleic acids, subintimal cell bodies are stained dark blue while the surrounding synovial extracellular matrix stains much lighter. This feature allows MATLAB to isolate subintimal cells from the background using

color and hue/saturation filters, correcting for the natural variance in the stain by using a red and green channel ratio. Once the cells were isolated, the script automatically calculates the number of cells, average cell density (# cells/100 pixels^2), average length of the major and minor axes of the cells, average cell aspect ratio (major axis/minor axis), and the percentage of cells within ±3 degrees of vertical alignment (with the vertical axis defined by the edge of the synovium).

Analysis of variance and post hoc assessments

For measures of ossification, subchondral edemas, and synovial cell morphology, results from the 4 graders were averaged to derive 72 representative animal means. For ETBA and TBA, data from multiple sections and multiple slides were averaged such that 72 animal means were calculated for the 2 graders. Then, the results from these 2 graders were averaged to derive 72 animal means. These animal means were used to assess differences between 9 treatments (naïve plus 8 separate surgery-time points) using a 1-way analysis of variance (ANOVA) followed by a Tukey's Honestly Significant Difference (HSD) post hoc test, when indicated. Significance levels were set as 0.05 for both tests. Furthermore, to assess inter-grader variability, intraclass correlation coefficients (ICCs) were calculated for each histological measure using SPSS Statistics 24 (alpha model with two-way random compensation).

Results

Ossification at the subchondral bone–cartilage interface

At 1 and 2 weeks after a simulated meniscus injury, significant ossification was observed at the subchondral bone–cartilage interface in the MMT group relative to naïve and MCLT sham procedures ($p < 0.025$). However, at weeks 4 and 6, similar levels of ossification were observed in the MMT and MCLT sham groups, despite a lack of articular cartilage remodeling in the MCLT sham group (Figure 4). Moreover, significant ossification was also observed in the MCLT sham group relative to the naive group at weeks 2, 4, and 6 post-surgery ($p < 0.013$).

Subchondral bone edema

Edemas only appeared in animals with simulated meniscal injury, and generally, only appeared at later time points (Figure 5). In MMT animals, the percentage of sections containing evidence of edema increased over time, indicated by weeks 2, 4, and 6MMT animals having a higher prevalence of edema than naïve controls and MCLT sham ($p < 0.0001$) and weeks 4 and 6 MMT animals having a higher prevalence than week 1 MMT animals ($p < 0.0001$). Edema size in MMT animals was also significantly larger than naïve controls and MCLT animals at week 6 post-surgery ($p < 0.0001$).

Epiphyseal trabecular bone area

At week 4, the overall ETBA increased in MMT animals relative to naïve controls ($p = 0.031$); however by week 6, both MMT and MCLT sham animals had increased ETBA relative to naïve animals ($p < 0.040$, Figure 6B). The increased ETBA in MMT animals may be largely influenced by ETBA in zones B1 and C1, which include the majority of ossified

cartilage (Figure 6C and D). In MMT animals, zone C1 area is larger than the respective naïve zone at all time points ($p < 0.043$), and zone B1 area is larger than the respective naïve zone at weeks 4 and 6 post-surgery ($p < 0.002$). Conversely, while the MCLT sham exhibited an increased overall ETBA at week 6, no significant zonal differences were found at any time points when compared to naïve.

Trabecular bone area

Overall, TBA measures exhibited similar results as found with the ETBA. At week 4, overall TBA in MMT animals was increased relative to naive animals ($p = 0.0005$). At week 6, TBA in both MMT and MCLT sham was increased relative to naive animals ($p < 0.0002$) with MMT TBA also larger than MMT TBA values at weeks 1 and 2 ($p < 0.004$, Figure 6F). Zones B1 and C1 TBA measures were also similar to ETBA results in which animals had increased zone B1 TBA at weeks 4 and 6 post-surgery relative to MCLT sham and naive animals ($p < 0.037$, Figure 6G) and increased zone C1 TBA at all time points relative to naive animals ($p < 0.001$) and MCLT sham animals at weeks 2, 4, and 6 ($p < 0.023$, Figure 6H). Additionally, at weeks 4 and 6 post-surgery, MMT animal zone C1 TBA was increased from MMT values at weeks 1 and 2 post-surgery ($p < 0.001$).

Synovial changes

In healthy animals, synovial subintimal fibroblasts qualitatively appeared as spindles with strong population directionality (Figure 7A). Conversely, cell bodies in the synovial stroma of MMT animals were more spherical and lacked directionality, and MCLT sham subintimal cell bodies were morphologically between naïve and MMT animals. As such, cell aspect ratio (a quantification of cell shape) was larger in naïve animals relative to MCLT sham and MMT animals ($p < 0.0001$, Figure 7C). These morphological changes to cell shape are perhaps best described by changes in the cell's major and minor axes lengths, where the major axis decreased in both MMT and MCLT animals across time, while the minor axis increased at 1 week post-surgery then trended back to naïve levels (Figure 7B and D). This plot clearly demonstrates the similar trend, but different levels of magnitude observed, in changes to the cell morphology in the MMT and MCLT sham animals.

Along with changes to cell morphology, a lower percentage of the synovial cell was aligned with the synovial edge in MMT animals relative to naïve controls at all time points ($p < 0.0001$, Figure 7E). Similarly, the percentage of cells that aligned with the synovial edge was lower in MCLT animals relative to naïve controls at weeks 2, 4, and 6 post-surgery ($p < 0.0001$). Though fewer cells were aligned in both MMT and MCLT sham animals, the percentage of the cell population that was aligned was significantly different between the MMT and MCLT sham animals at week 6 post-surgery ($p = 0.031$).

Finally, subintimal cell density of MMT animals was substantially larger than naïve animals at all time points even after correcting for image size ($p < 0.0001$, Figure 7F). Similarly, subintimal cell density of MCLT sham animals was larger than naive animals at weeks 2, 4, and 6 post-surgery ($p < 0.002$), though not as large as MMT animals at week 6 ($p = 0.003$).

Intra-class correlation coefficients

Overall ICCs for all histological measures were above 0.89 with ICCs calculated for measures of subintimal cell density, presence of edema, ossification width, TBA, and ETBA above 0.95 (Table 2).

Discussion

Following meniscal injury, post-traumatic OA affects all tissues within a joint. Structural changes include cartilage lesion formation, changes in subchondral bone density, formation of osteophytes along the joint margin, and fibrosis and thickening of the synovium. Additionally, inflammation chronically alters the joint at the molecular level, disrupting joint homeostasis and promoting catabolic disease processes. Most histological assessments of OA in rodents do not describe changes throughout the joint, but instead focus on cartilage damage alone. Exploring ways to quantify OA-related changes in these other tissues can provide new insights to the totality of OA pathogenesis following meniscal injury.

While the OARSI scheme dedicated one measure to synovial changes (capsular thickness), the subintimal cell morphology measures presented in this study add detail that may not be captured by capsular thickness alone. Moreover, our data indicate synovial cells in the subintimal layer have a sensitive, graded response to injury and might provide a useful indicator of joint health. Not only were MMT and MCLT sham subintimal cells different from naïve, their morphologies were distinct from one another and continued to change at each time point. These data were measured from a synovial location suggested by the OARSI scheme for rats, but other synovial locations may offer additional insight to synovial changes resulting from meniscal injury.

The OARSI histopathology scheme for rats recommends toluidine blue stain to assess OA-related cartilage, bone, and synovial damage; however, cell morphology is not typically evaluated with this stain. However, in this manuscript, cell morphology changes were successfully measured using toluidine blue. Nonetheless, the low contrast between the cell bodies and the surrounding tissue, combined with natural variance in the dye, do present some challenges. Toluidine blue can appear purple when underexposed and blue when overexposed, requiring unique color thresholds to be used for each histological image. This variation can obscure accurate cell identification and may result in batch-to-batch variations. Our script partially addresses this challenge by using a red-to-green channel ratio, but better image analysis could increase the sensitivity of this measure. Additionally, other stains, such as hematoxylin & eosin, may increase precision, though at the cost of assessing other tissue features on the same section. Recognizing that OA is a whole joint disease affecting multiple tissues, assessing tissue damage on the same section is ideal. Thus, our approach using toluidine blue allows observable structural changes for the majority of tissue within a joint to be assessed, along with observations of cell morphology.

Subchondral bone is a complex network of marrow voids and trabecular bone. On histological slides, little order can be visually identified in subchondral bone, with patterns changing drastically from slide to slide, and occasionally section to section. Using CT scans, subchondral bone has been shown to become more dense in human OA (25–28). Increases in

subchondral bone density have also been observed in rodents using a μCT (29–31) and ultrasound (32,33). Using histology from a similar rodent OA model, another study measured TBA according to the ASBMR histomorphometry nomenclature committee (16). In that study, TBA was measured by imaging a 600 × 800 μm portion of subchondral bone from two slides located 100 μm apart. Trabecular bone volumes calculated from these two images were then combined to represent a single trabecular bone volume for each joint. This approach was not sensitive enough to detect increasing bone area in our model (data not shown); however, expanding this approach to three consecutive images from three sequential slides (9 total) was enough to confirm that subchondral bone changes were occurring in MMT and MCLT animals.

Many histological scoring methods are typically performed by averaging results from multiple graders (11,34–39) or multiple sections (22–24,30,39). This approach is often chosen to mitigate the high variability and subjectivity of most scoring methods. In this manuscript, several measures of subchondral bone and synovial cell morphology are automated and will consistently produce the same result given the same image input, thus reducing the need for multiple graders or histological images. However, the manually chosen measures defining ossification may also contain some variability and subjectivity, but less severe than traditional scoring methods. In traditional scoring methods, the full range of tissue degeneration is contained in relatively few, discrete values. Conversely, the quantitative ossification measures described in this manuscript are continuous and allow for a more precise description of tissue degeneration.

While analyzing subchondral bone area through histology is not as rapid or precise as μCT, the histological approach presented herein was still able to collect spatial and structural data from cartilage, bone, and synovium from the same section. This work was also limited to using slides near the cartilage lesion to assess subchondral bone changes, but could be expanded to other joint locations as other studies have shown for trabecular bone volume changes in other areas (31,40,41).

During OA-related ossification, cartilage at the osteochondral interface increasingly calcifies, decreasing cartilage thickness and increasing trabecular bone thickness (15,42,39,43); thus, ossification could be responsible for the increased area of bone in MMT and MCLT sham groups relative to naïve. Comparisons of TBA in zones B1 and C1 revealed significant differences between the MMT animals and naïve animals at all time points; however, no local differences were found between MCLT animals and naïve controls. This finding may indicate that bony remodeling is occurring over the entire medial subchondral bone compartment in MCLT sham animals, while changes in the MMT animal may be focally related to the cartilage lesion.

The bone and synovium measures presented in this work describe joint damage not widely assessed after a simulated medial meniscus injury in the rat. Moreover, these bony and synovial changes are quantitative and continuous. Overall, these data demonstrate that OA affects the joint as an organ system, and through quantification of changes throughout the entire joint, a better understanding of the pathogenesis of joint destruction may be constructed.

Acknowledgments

The histological data could not have been collected without contributions from Ms. Brittany Jacobs, Ms. Emily Lakes, and Mr. Yash Shah, and their contributions are greatly appreciated.

Funding

Research reported in this publication was supported by the National Institute of Arthritis and Musculoskeletal and Skin Diseases (NIAMS) of the National Institutes of Health under award numbers K99/R00AR057426.

References

1. Englund P, Lohmander L. Risk factors for symptomatic knee osteoarthritis fifteen to twenty-two years after meniscectomy. Arthritis Rheumatol. 2004; 50(9):2811–2819.
2. Lohmander L, Englund P, Dahl L, Roos E. The long-term consequence of anterior cruciate ligament and meniscus injuries osteoarthritis. Am J Sports Med. 2007; 35(10):1756–1769. [PubMed: 17761605]
3. Felson DT. Osteoarthritis as a disease of mechanics. Osteoarthr Cartil. 2013; 21(1):10–15. [PubMed: 23041436]
4. Loeser RF, Goldring SR, Scanzello CR, Goldring MB. Osteoarthritis: A disease of the joint as an organ. Arthritis Rheum. 2012; 64(6):1697–1707. [PubMed: 22392533]
5. Janusz M. Induction of osteoarthritis in the rat by surgical tear of the meniscus: Inhibition of joint damage by a matrix metalloproteinase inhibitor. Osteoarthr Cartil. 2002; 10(10):785–791. [PubMed: 12359164]
6. Glasson SS, Blanchet TJ, Morris EA. The surgical destabilization of the medial meniscus (DMM) model of osteoarthritis in the 129/SvEv mouse. Osteoarthr Cartil. 2007; 15(9):1061–1069. [PubMed: 17470400]
7. Gerwin N, Bendele AM, Glasson S, Carlson CS. The OARSI histopathology initiative: Recommendations for histological assessments of osteoarthritis in the rat. Osteoarthr Cartil. 2010; 18(Suppl 3):S24–S34.
8. Kraus VB, Huebner JL, DeGroot J, Bendele A. The OARSI histopathology initiative: Recommendations for histological assessments of osteoarthritis in the guinea pig. Osteoarthr Cartil. 2010; 18(Suppl 3):1–38. [PubMed: 19737530]
9. McIlwraith C, Frisbie D, Kawcak C, Fuller C, Hurtig M, Cruz A. The OARSI histopathology initiative: Recommendations for histological assessments of osteoarthritis in the horse. Osteoarthr Cartil. 2010; 18(Suppl 3):S93–S105. [PubMed: 20864027]
10. Little C, Smith M, Cake M, Read R, Murphy M, Barry F. The OARSI histopathology initiative: Recommendations for histological assessments of osteoarthritis in sheep and goats. Osteoarthr Cartil. 2010; 18(Suppl 3):S80–S92. [PubMed: 20864026]
11. van der Sluijs JA, Geesink RG, van der Linden AJ, Bulstra SK, Kuyer R, Drukker J. The reliability of the Mankin score for osteoarthritis. J Orthop Res. 1992; 10(1):58–61. [PubMed: 1727936]
12. Glasson S, Chambers M, Van Den Berg W, Little C. The OARSI histopathology initiative: Recommendations for histological assessments of osteoarthritis in the mouse. Osteoarthr Cartil. 2010; 18(Suppl 3):S17–S23.
13. Pritzker KPH, Gay S, Jimenez SA, Ostergaard K, Pelletier JP, Revell K, Salter D, van den Berg WB. Osteoarthritis cartilage histopathology: Grading and staging. Osteoarthr Cartil. 2006; 14(1): 13–29. [PubMed: 16242352]
14. Grynpas M, Alpert B, Katz I, Lieberman I, Pritzker K. Subchondral bone in osteoarthritis. Calcif Tissue Int. 1991; 49:20–26. [PubMed: 1893292]
15. Mahjoub M, Berenbaum F, Houard X. Why subchondral bone in osteoarthritis? The importance of the cartilage bone interface in osteoarthritis. Osteoporos Int. 2012; 23(Suppl 8):S841–S846. [PubMed: 23179566]
16. Hayami T, Pickarski M, Wesolowski GA, McLane J, Bone A, Destefano J, Rodan GA, Duong LT. The role of subchondral bone remodeling in osteoarthritis: Reduction of cartilage degeneration and

prevention of osteophyte formation by alendronate in the rat anterior cruciate ligament transection model. Arthritis Rheum. 2004; 50(4):1193–1206. [PubMed: 15077302]

17. de Lange-Brokaar BJE, Ioan-Facsinay A, van Osch GJVM, Zuurmond A-M, Schoones J, Toes REM, Huizinga TW, Kloppenburg M. Synovial inflammation, immune cells and their cytokines in osteoarthritis: A review. Osteoarthr Cartil. 2012; 20(12):1484–1499. [PubMed: 22960092]
18. Kloefkorn HE, Jacobs BY, Loye AM, Allen KD. Spatiotemporal gait compensations following medial collateral ligament and medial meniscus injury in the rat: Correlating gait patterns to joint damage. Arthritis Res Ther. 2015; 17(1):287. [PubMed: 26462474]
19. Allen KD, Mata BA, Gabr MA, Huebner JL, Adams SB, Kraus VB, Schmitt DO, Setton LA. Kinematic and dynamic gait compensations resulting from knee instability in a rat model of osteoarthritis. Arthritis Res Ther. 2012; 14(2):R78. [PubMed: 22510443]
20. Bove SE, Laemont KD, Brooker RM, Osborn MN, Sanchez BM, Guzman RE, Hook KE, Juneau PL, Connor JR, Kilgore KS. Surgically induced osteoarthritis in the rat results in the development of both osteoarthritis-like joint pain and secondary hyperalgesia. Osteoarthr Cartil. 2006; 14(10): 1041–1048. [PubMed: 16769229]
21. Mapp PI, Walsh DA, Bowyer J, Maciewicz RA. Effects of a metalloproteinase inhibitor on osteochondral angiogenesis, chondropathy and pain behavior in a rat model of osteoarthritis. YJOCA. 2010; 18(4):593–600.
22. Dempster D, Compston J, Drezner M, Glorieux F, Kanis J, Malluche H, Meunier PJ, Ott SM, Recker RR, Parfitt AM. Standardized nomenclature, symbols, and units for bone histomorphometry: A 2012 update of the report of the ASBMR histomorphometry nomenclature committee. J bone Miner Res. 2013; 20(2):233–243.
23. Parfitt AM, Drezner MK, Glorieux FH, Kanis JA, Malluche H, Meunier PJ, Ott SM, Recker RR. Bone histomorphometry: Standardization of nomenclature, symbols, and units. Report of the ASBMR Histomorphometry Nomenclature Committee. J Bone Miner Res. 1987:595–610. [PubMed: 3455637]
24. Bobinac D, Spanjol J, Zoricic S, Maric I. Changes in articular cartilage and subchondral bone histomorphometry in osteoarthritic knee joints in humans. Bone. 2003; 32(3):284–290. [PubMed: 12667556]
25. Intema F, Thomas T, Anderson D, Elkins J, Brown T, Amendola A, Lafeber FP, Saltzman CL. Subchondral bone remodeling is related to clinical improvement after joing distraction in the treatment of ankle osteoarthritis. Osteoarthr Cartil. 2011; 72(2):181–204.
26. Turmezei TD, Poole KES. Computed tomography of subchondral bone and osteophytes in hip osteoarthritis: The shape of things to come? Front Endocrinol (Lausanne). 2011; 2(Dec):1–9. [PubMed: 22649356]
27. Li G, Yin J, Gao J, Cheng TS, Pavlos NJ, Zhang C, Zheng MH. Subchondral bone in osteoarthritis: Insight into risk factors and microstructural changes. Arthritis Res Ther. 2013; 15(223)doi: 10.1186/ar4405
28. Swagerty DL, Hellinger D. Radiographic assessment of osteoarthritis. Am Fam Phys. 2001; 64(2): 279–286.
29. McErlain DD, Ulici V, Darling M, Gati JS, Pitelka V, Beier F, Holdsworth DW. An in vivo investigation of the initiation and progression of subchondral cysts in a rodent model of secondary osteoarthritis. Arthritis Res Ther. 2012; 14(1):R26. [PubMed: 22304985]
30. Mohan G, Perilli E, Parkinson IH, Humphries JM, Fazzalari NL, Kuliwaba JS. Pre-emptive, early, and delayed alendronate treatment in a rat model of knee osteoarthritis: Effect on subchondral trabecular bone microarchitecture and cartilage degradation of the tibia, bone/cartilage turnover, and joint discomfort. Osteoarthr Cartil. 2013; 21(10):1595–1604. [PubMed: 23827368]
31. McErlain DD, Appleton CTG, Litchfield RB, Pitelka V, Henry JL, Bernier SM, Beier F, Holdsworth DW. Study of subchondral bone adaptations in a rodent surgical model of OA using in vivo micro-computed tomography. Osteoarthr Cartil. 2008; 16(4):458–469. [PubMed: 17900933]
32. Saïed A, Chérin E, Gaucher H, Laugier P, Gillet P, Floquet J, Netter P, Berger G. Assessment of articular cartilage and subchondral bone: Subtle and progressive changes in experimental osteoarthritis using 50 MHz echography in vitro. J bone Miner Res. 1997; 12(9):1378–1386. [PubMed: 9286753]

33. Saarakkala S, Waris P, Waris V, Tarkiainen I, Karvanen E, Aarnio J, Koski JM. Diagnostic performance of knee ultrasonography for detecting degenerative changes of articular cartilage. Osteoarthr Cartil. 2012; 20(5):376–381. [PubMed: 22343004]
34. Beckett J, Jin W, Schultz M, Chen A, Tolbert D, Moed BR, Zhang Z. Excessive running induces cartilage degeneration in knee joints and alters gait of rats. J Orthop Res. 2012; 30(10):1604–1610. [PubMed: 22508407]
35. Hunter DJ, Lo GH, Gale D, Grainger AJ, Guermazi A, Conaghan PG. The reliability of a new scoring system for knee osteoarthritis MRI and the validity of bone marrow lesion assessment: BLOKS (Boston Leeds Osteoarthritis Knee Score). Ann Rheum Dis. 2008; 67(2):206–211. [PubMed: 17472995]
36. Krenn V, Morawietz L, Burmester G-R, Kinne RW, Mueller-Ladner U, Muller B, Haupl T. Synovitis score: Discrimination between chronic low-grade and high-grade synovitis. Histopathology. 2006; 49(4):358–364. [PubMed: 16978198]
37. Panahifar A, Jaremko JL, Tessier AG, Lambert RG, Maksymowych WP, Fallone BG, Doschak MR. Development and reliability of a multi-modality scoring system for evaluation of disease progression in preclinical models of osteoarthritis: Celecoxib may possess disease-modifying properties. Osteoarthr Cartil. 2014; 22(10):1639–1650. [PubMed: 25278073]
38. Custers RJH, Creemers LB, Verbout AJ, van Rijen MHP, Dhert WJa, Saris DBF. Reliability, reproducibility and variability of the traditional histologic/histochemical grading system vs the new OARSI osteoarthritis cartilage histopathology assessment system. Osteoarthr Cartil. 2007; 15(11):1241–1248. [PubMed: 17576080]
39. Cox LGE, Donkelaar CC, Van Rietbergen B, Van Emans PJ, Ito K. Alterations to the subchondral bone architecture during osteoarthritis: Bone adaptation vs endochondral bone formation. Osteoarthr Cartil. 2013; 21:331–338. [PubMed: 23142725]
40. Gu XI, Palacio-Mancheno PE, Leong DJ, Borisov YA, Williams E, Maldonado N, Lauder D, Majeska RJ, Schaffler MB, Sun HB, Cardoso L. High resolution micro arthrography of hard and soft tissues in a murine model. Osteoarthr Cartil. 2012; 20(9):1011–1019. [PubMed: 22613702]
41. Mohan G, Perilli E, Kuliwaba JS, Humphries JM, Parkinson IH, Fazzalari NL. Application of in vivo micro-computed tomography in the temporal characterisation of subchondral bone architecture in a rat model of low-dose monosodium iodoacetate-induced osteoarthritis. Arthritis Res Ther. 2011; 13(6):R210. [PubMed: 22185204]
42. Pap T, Korb-pap A. Cartilage damage in osteoarthritis and rheumatoid arthritis: Two unequal siblings. Nat Publ Gr. 2015; 11(10):606–615.
43. Schultz M, Molligan J, Schon L, Zhang Z. Pathology of the calcified zone of articular cartilage in post-traumatic osteoarthritis in rat knees. PLoS One. 2015; 10(3):1–12.

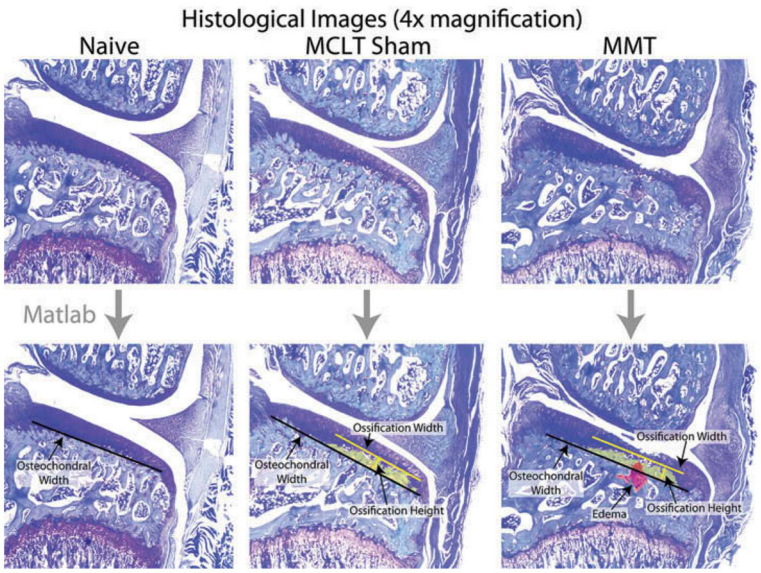

Figure 1.

Summary of MATLAB script to measure changes at the subchondral bone-cartilage interface following a simulated meniscus injury in the rat. Once loaded, users place markers defining osteochondral width by clicking the two end points defining the measure (black line). If present, the user then outlines any edemas (red) or ossification (yellow) present in the subchondral bone using a series of clicks.

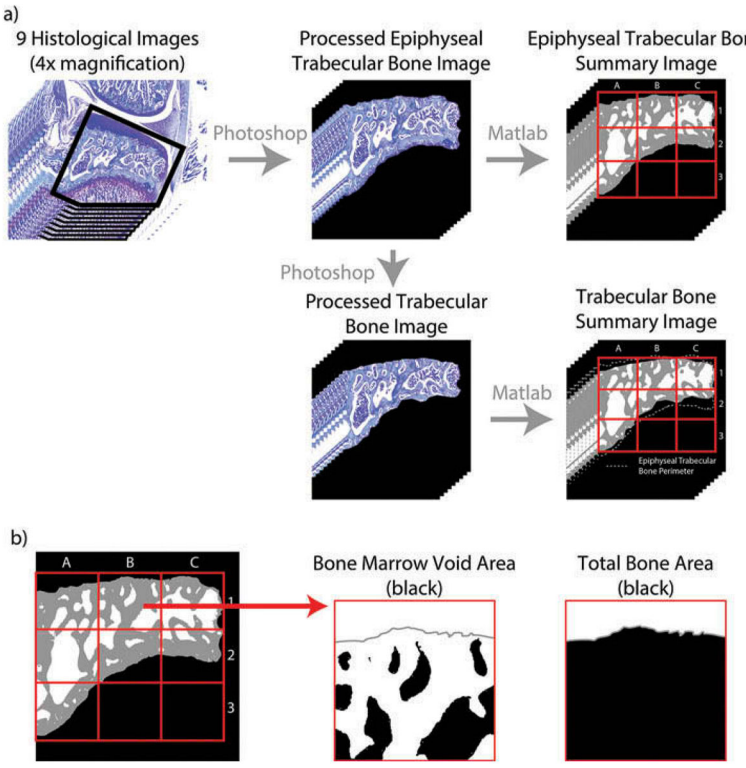

Figure 2.

Calculating trabecular bone area. a) The image is first prepared in Adobe Photoshop by rotating the image such that the tibial plateau is horizontal and erasing any points where the dehydrated bone marrow is contiguous with the trabecular bone. To prepare the epiphyseal trabecular bone images, surrounding tissue is then removed leaving the subchondral bone area between the articular cartilage and epiphyseal plane. From these images, the trabecular bone images are created by removing the bone between the articular cartilage and bone marrow voids and between the epiphyseal plane and bone marrow voids. b) This Photoshop prepared image is then loaded into a custom MATLAB script, where trabecular bone area is calculated over the entire subchondral bone area and within 9 pre-defined zones (red grid).

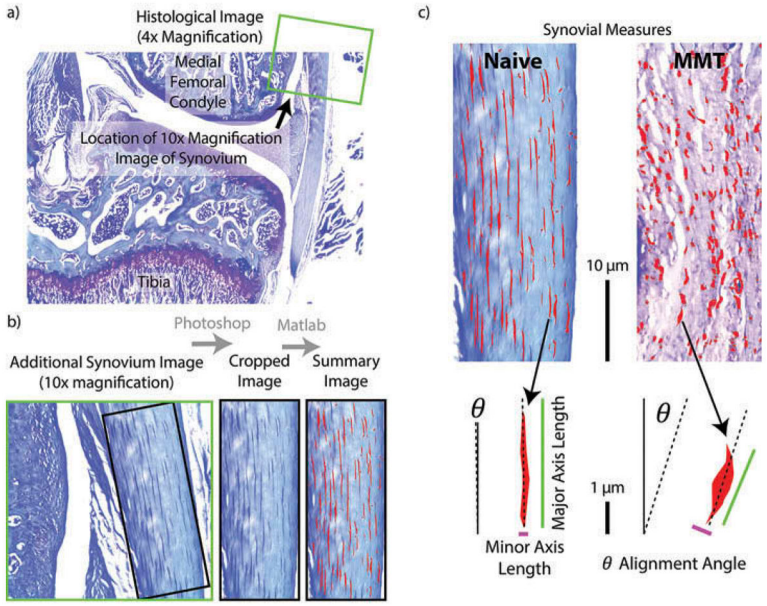

Figure 3.

Calculating synovium measures. a) The 10x magnification synovial image (green square) is taken proximal to the meniscus in the medial compartment. b) As in Figure 2, the synovial image is first prepared in Adobe Photoshop by rotating the image to vertical and cropping the image such at only synovial tissue is included. c) This Photoshop prepared image is then loaded into a custom MATLAB script, where subintimal cells are identified and measures of cellular density and morphology are calculated.

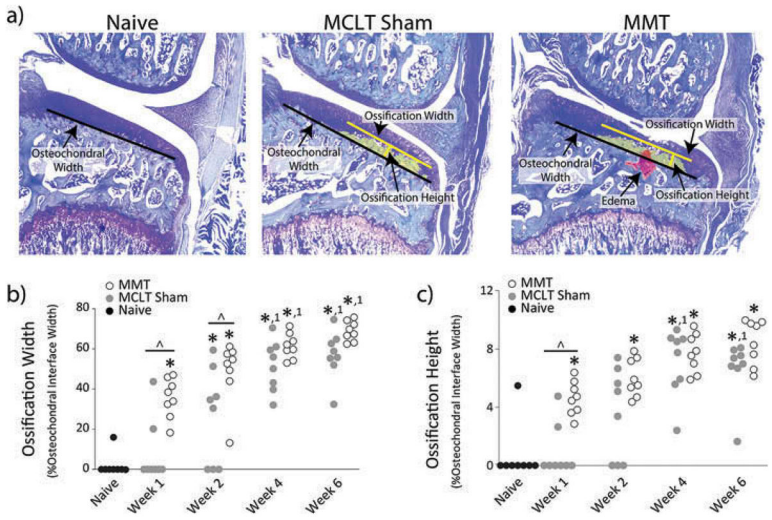

Figure 4.

Ossification of Subchondral Bone. a) Representative toluidine blue-stained images from naïve, MCLT sham, and MMT groups. b) and c) Ossification occurs in both MMT and MCLT Sham animals and becomes progressively more severe. Data are shown as animal averages. * denotes significance from naïve; ^ denotes significance from MCLT Sham values at respective time point; [1] denotes significance from respective group at week 1 post-surgery.

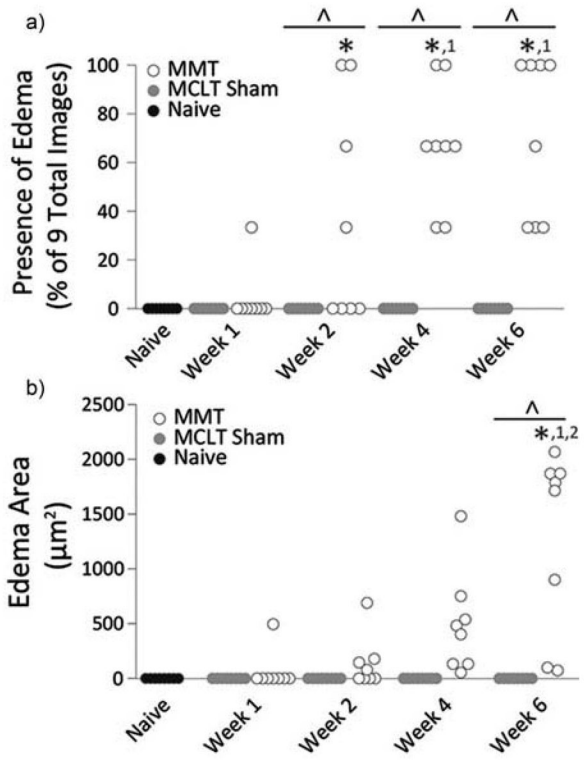

Figure 5.

Edema Measures. a) Edema appeared in some MMT animals as early as week 1 but occurred in all MMT animals by week 4. b) Edema area is relatively small in MMT animals until week 6. Data are shown as animal averages. *denotes significance from naïve; ^denotes significance from MCLT Sham values at respective time point; [1]denotes significance from respective group at week 1 post-surgery; [2]denotes significance from respective group at week 2 post-surgery.

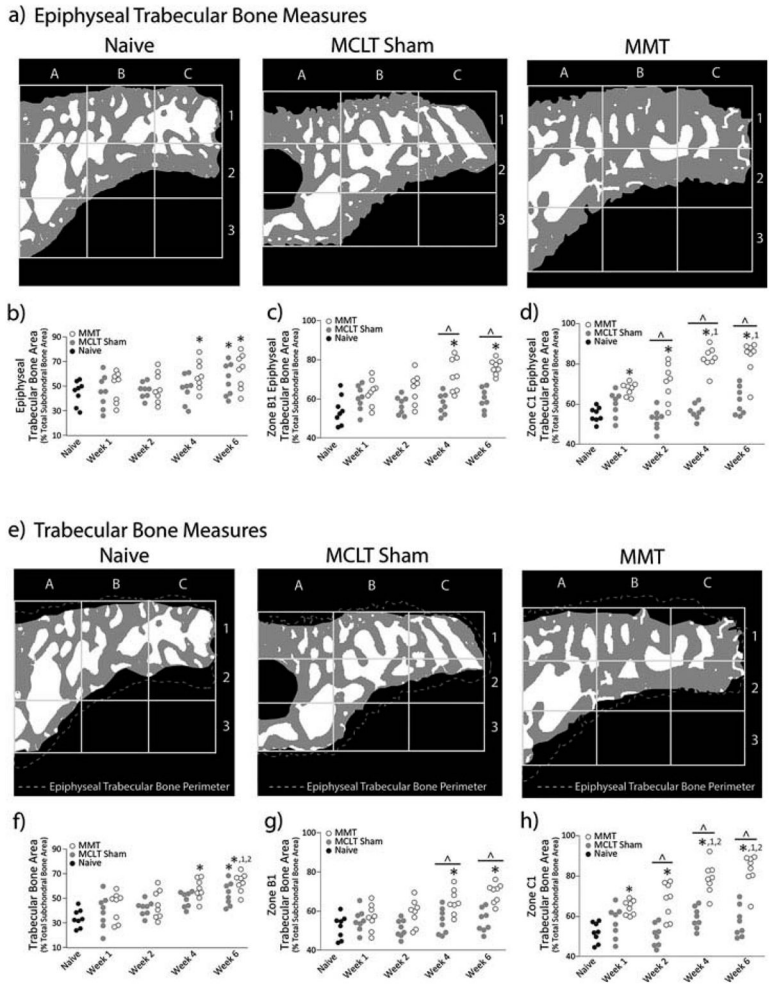

Figure 6.

Trabecular Bone Area. a) Representative images of processed epiphyseal trabecular bone area bone (ETBA) images for naïve, MCLT sham, and MMT groups. b) ETBA increases in MMT animals by week 4 post-surgery and in MCLT animals by week 6 post-surgery. c) At later time points, zone B1 ETBA in MMT animals is significantly larger than both MCLT Sham and naïve animals. d) Zone C1 ETBA increases progressively in MMT animals only. Zone C1 ETBA is larger in MMT animals relative to naïve animals at all time points and larger than MCLT sham animals at weeks 2, 4, and 6 post-surgery. e) Representative images of processed trabecular bone area bone (TBA) images for naïve, MCLT sham, and MMT groups. f) TBA increases in MMT animals by week 4 post-surgery and in MCLT animals by week 6 post-surgery. g) At later time points, zone B1 TBA in MMT animals is significantly larger than both MCLT Sham and naïve animals. h) Zone C1 TBA increases progressively in MMT animals only. Zone C1 TBA is larger in MMT animals relative to naïve animals at all time points and larger than MCLT sham animals at weeks 2, 4, and 6 post-surgery. Data are shown as animal averages. * denotes significance from naïve; ^ denotes significance from MCLT Sham values at respective time point; [1] denotes significance from respective group at week 1 post-surgery; [2] denotes significance from respective group at week 2 post-surgery.

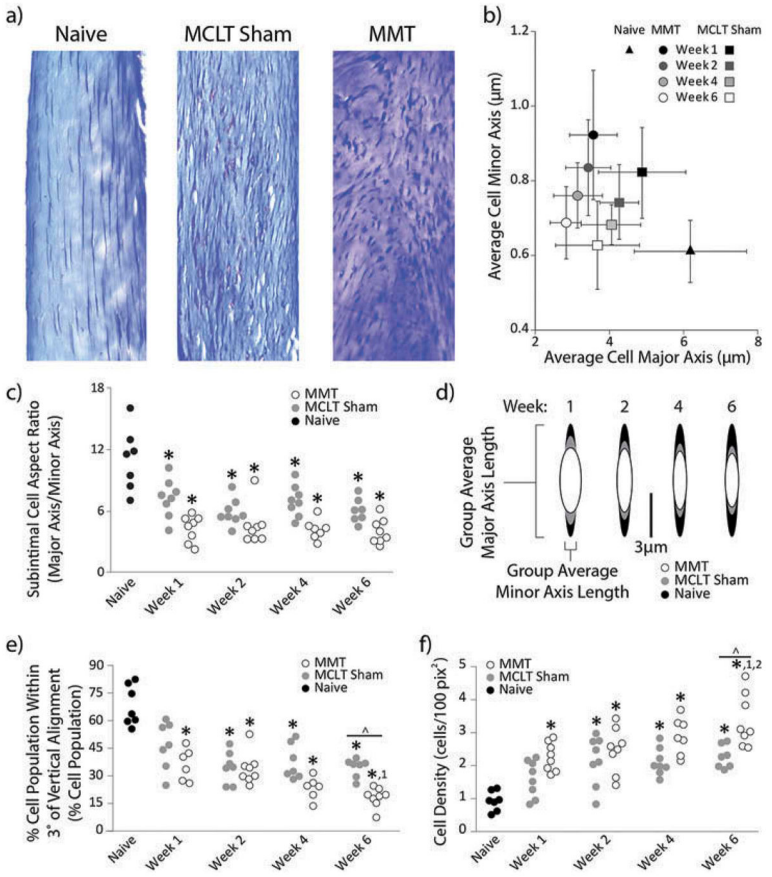

Figure 7.

Subintimal cell morphology. a) Representative cropped and rotated histological images of synovium stained with toluidine blue. b) Group averages and standard deviations of cell minor axis plotted against cell major axis. In MMT animals, minor axis measures increase and major axis measures decrease. There is also a trend for the major axis to progressively reduce across time points. c) MMT and MCLT sham animal subintimal cell aspect ratio are lower than naïve animals at all time points. d) Graphical representation of cell shape from group averages of major and minor axis length at each time point. e) Progressively lower percentages of subintimal cell population are aligned in both MMT and MCLT Sham animals. f) Cell proliferation, indirectly measured as cell density, increased progressively in both MMT and MCLT Sham groups, though the effect in MMT animals was more significant than MCLT Sham animals by week 6 post-surgery. Data are shown as animal averages. * denotes significance from naïve; ^ denotes significance from MCLT Sham values at respective time point; [1] denotes significance from respective group at week 1 post-surgery; [2] denotes significance from respective group at week 2 post-surgery.

Table 1

Definitions of Subchondral Bone and Synovium Measures.

Histological measure	Unit	Definition
Ossification width	%	$\frac{Width\ of\ Ossification\ Area}{Width\ of\ Osteochondral\ Interface}$
Ossification height	%	$\frac{Width\ of\ Ossification\ Area}{Width\ of\ Osteochondral\ Interface}$
Edema area	μm^2	*Sum of the Area Covered by Edema*
Edema presence	%	$\frac{Number\ of\ 9\ Medical\ Compartment\ Images\ Containing\ Edema}{9}$
Epiphyseal trabecular bone area (ETBA)	%	$\frac{Sum\ of\ Area\ Covered\ by\ Trabecular\ Bone\ Between\ Articlar\ Cartilage\ and\ Epiphyseal\ pl}{Sum\ of\ Area\ Covered\ by\ Trabecular\ Bone+Bone\ Marrow\ Voids\ Articlar\ Cartilage\ and\ Epiphy}$
Trabecular bone area (TBA)	%	$\frac{Sum\ of\ Area\ Covered\ by\ Trabecular\ Bone}{Sum\ of\ Area\ Covered\ by\ Trabecular\ Bone+Bone\ Marrow\ Voids}$
Synovial subintimal cell density	$\frac{cells}{100\ pixels^2}$	$\left(\frac{Number\ of\ Cells\ in\ Image}{Image\ Width\times Image\ Height}\right)\times 100$
Synovial subintimal cell aspect ratio	Unitless	$\frac{Cell\ Major\ Axis\ Length}{Cell\ Minor\ Axis\ Length}$
Synovial subintimal cell alignment	% cell population	$\frac{Number\ of\ Cells\ within\pm 3^\circ\ of\ Vertical\ Alignment}{Number\ of\ Cells\ in\ Image}$

Table 2

Intraclass Correlation Coefficients (ICCs).

Histological measure	ICC
Synovial subintimal cell aspect ratio	0.901
Synovial subintimal cell density	0.953
% Synovial subintimal cell population within ±3° of vertical alignment	0.917
Presence of edema on 9 total images	0.999
Edema area	0.895
Ossification width	0.951
Ossification height	0.892
Trabecular bone area	0.961
Epiphyseal trabecular bone area	0.974